ACS OMEGA

http://pubs.acs.org/journal/acsodf

Article

Forensic Discrimination of Drug Powder Based on Drug Mixing Condition Determined Using Micro Fourier Transform Infrared Spectroscopy

Takahiro Iwai, Sadao Honda, Shimpei Watanabe, Ritsuko Matsushita, Toshio Nakanishi, Masahisa Takatsu, Taro Moriwaki, Makina Yabashi, Tetsuya Ishikawa, and Yasuo Seto*

Cite This: *ACS Omega* 2023, 8, 4285−4293

Read Online

ACCESS | Metrics & More | Article Recommendations | Supporting Information

ABSTRACT: The quantitative evaluation of the drug mixing condition was conducted for application in the forensic discrimination of drug powders using micro Fourier transform infrared (FT-IR) spectroscopy. Bromhexine hydrochloride (BHCl) and *p*-hydroxybenzoic acid (PHBA) were used as the simulated drug and additive, respectively. Equal masses of two chemicals were (1) simply mixed, (2) homogenized using agate mortar, or (3) dissolved in methanol and dried, and then (4) homogenized using agate mortar. The mixed powders dispersed on BaF_2 plates were subjected to mapping analysis of micro FT-IR spectroscopy using synchrotron radiation (SR) or globar light in transmission mode with aperture sizes of 2.5 x 2.5 and 10 x 10 μm^2, and $x-y$ scanning steps of 2.5 and 10 μm, respectively. The areas of the vibration bands specific to BHCl (C−N bending) and PHBA (C═O stretching) were converted to the molar contents (C_{BHCl}, C_{PHBA}), and the relative content ratio (RCR: $C_{PHBA}/[C_{BHCl} + C_{PHBA}]$) was used as one mixing parameter. The resulting two-dimensional distribution map provided the relative spatial localizations of the two species, and frequency histograms with a horizontal axis of RCR were plotted to evaluate the RCR distribution. The percentage frequency of the extreme value in which RCR was 0 or 1 (%EV) was used as one mixing index. After excluding the extreme values, the coefficient of variation (CV) of the RCR distribution was used as another mixing index. The differentiation among four mixing modes could be evaluated from the standpoint of %EV and CV, and the discrimination capacity by SR instrument was superior to that by globe light instrument.

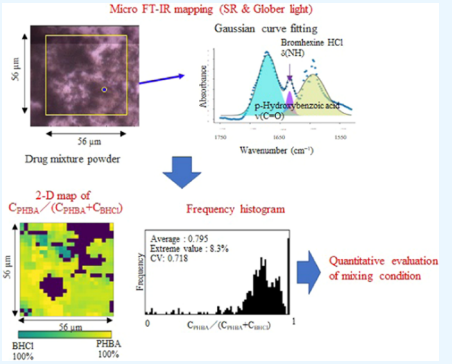

INTRODUCTION

Drug abuse is currently prevalent,[1] and forensic examination is performed by national and local law enforcement authorities to counter this serious problem.[2] In the field of forensic drug analysis, forensic chemistry involves analysis of a seized specimen to identify illegal drugs and yield any other data. Discrimination among seized drug specimens is critical to elucidate connections between seizures based on the synthetic route, enabling one to deduce the distribution chain: drug manufacturers, sources of supply, and trafficking routes. In addition to the main illicit drug identification via gas or liquid chromatography−mass spectrometry (GC- or LC-MS), numerous other types of analyses are performed,[3,4] including chiral analysis and stable isotope ratio mass spectrometry of the illicit drugs and impurity profiling of minor organic and inorganic components.[5] Evaluation of similarity is mainly performed based on the percentage contents, chiralities, and stable isotopic ratios of the illicit drugs, and GC profiles of minor organic impurities according to the Euclidean distances.[3] However, in numerous cases, the seized drug specimens cannot be discriminated due to a high similarity in characteristics determined using these methods. Moreover, within the same seized drug package, samples removed from different portions exhibit different isotope ratio mass spectra.[4] Not only illicit drug isotope ratios but also the contents of the other components[6] are highly likely to vary throughout the specimen. This may be ascribed to inhomogeneous mixing of the respective components due to manufacturing, trafficking, and distribution processes. Even with identical compositions, drug samples may be differentiated by the difference in mixing conditions during drug manufacturing. We aim to develop a novel mixing index for use in forensic discrimination to quantitatively evaluate the mixing conditions of seized drugs.

Imaging technology[7] is a basic means of obtaining distribution data of organic components in solid materials. Microscopic observation is the basic method but is inadequate because drug components cannot generally be discriminated by observing microscopic shapes and colors. Noninvasive

Received: November 26, 2022
Accepted: January 6, 2023
Published: January 17, 2023

spectroscopic chemical imaging yields valuable data,[8] with Raman spectroscopy also used in examining the spatial distribution of the components.[9] Micro Fourier transform infrared (FT-IR) spectroscopy is most frequently employed in numerous research fields,[8] including forensic science,[10] and used to visualize the ridge lines of latent fingerprints[11] and detect exogenous materials in fingerprints.[12] Drugs were identified in unknown pharmaceutical tablets[13] and various samples,[14,15] and explosives were identified using post-blast residues.[16] Micro FT-IR spectroscopy is generally utilized in screening and subsequent pinpoint identification of low levels of specific components, which are unevenly distributed in solid samples and undetected using bulk FT-IR spectroscopy. Yonemochi et al.[17] observed the dispersion of racemic compounds in pharmaceutical granules. Shinzawa et al. analyzed the co-localization of two polymers in heterogeneous resin using two-dimensional (2D) disrelation mapping of shifted FT-IR spectra caused by molecular interactions.[18] Okada et al. evaluated the dispersion of additives in polymer composites.[19] The coefficients of variation (CVs) in the distributions of the relative additive contents were plotted against the size of the measuring window, with the shape of the slope potentially indicating the mixing conditions. de Oliveira and de Juan developed a method of evaluating the heterogeneity indices of pharmaceutical blend quality using near-infrared hyperspectral imaging (0.1 × 0.1 mm^2 pixels) followed by variographic analysis, yielding the global heterogeneity and distribution uniformity indices.[20] However, these methods focus on the dispersion of one chemical component (or spectroscopically different chemical complex) and do not yield data regarding the mixing condition of two components.

As for the light source in FT-IR spectroscopy, synchrotron radiation (SR), which is used in FT-IR spectroscopy[21−23] and micro FT-IR spectroscopic imaging,[22,24−28] is superior to globar light in terms of light intensity resulting in apparent spatial resolution.[29−33] Attenuated total reflection (ATR) micro FT-IR spectroscopy, which is applied in various research fields, may be available to increase spatial resolution.[13,34,35]

Here, bromhexine hydrochloride (BHCl) and *p*-hydroxybenzoic acid (PHBA) were used as a model illicit drug and impurity component, respectively, and various mixing modes, such as simple powder mixing and agate mortar homogenization, were examined via mapping analysis of micro FT-IR spectroscopy using SR and globar light instruments. In analyzing the micro FT-IR spectroscopic data, the relative content ratio (RCR) of the two species was adopted as a mixing parameter, and 2D distribution maps and the related RCR frequency histograms were plotted based on quantitative evaluation of the mixing conditions. The superiority of the SR light source, with increased light intensity resulting in higher apparent spatial resolution, was confirmed in differentiating the various mixing modes.

EXPERIMENTAL SECTION

Materials. PHBA, KBr block crystals, KH_2PO_4, and methanol for use in LC-MS were purchased from FUJIFILM Wako Pure Chemical (Osaka, Japan), and BHCl was purchased from Sigma-Aldrich (St. Louis, MO). The water (<18.2 MΩ·cm) used in the study was purified using an Ultrapure Water System Type ω (Organo, Tokyo, Japan).

Sample Preparation. Mixtures of equal masses of PHBA and BHCl were prepared via the four mixing modes described below and used as samples (No. 1−4). (No. 1) Simple mixing: the respective powders were combined and mixed using a test tube mixer. (No. 2) Homogenizing in an agate mortar: the combined powder was ground thoroughly using an agate mortar and pestle for 3 min. (No. 3) Methanol dissolution and drying: the combined powder was dissolved in methanol, which was then evaporated on a hot plate at 40 °C. (No. 4) Homogenizing using an agate mortar after methanol dissolution-drying: The No. 3 mixture was ground thoroughly using an agate mortar and pestle for 3 min. A small amount of the mixture (approximately 1 mg) was placed directly on a BaF_2 disk (10 mmϕ, 1 mm thickness, OKEN, Tokyo, Japan) for use in micro FT-IR spectroscopy in transmission mode. After the sample preparation, they were preserved in a desiccator. After micro FT-IR spectroscopic measurement of the mixture, the water-related absorbance peaks around 1600 and 3800 cm^{-1} were not observed. We could not ascertain the obvious hygroscopicity of PHBA and BHCl.

To determine the IR absorption coefficients of the individual species, PHBA and BHCl were respectively ground with KBr block crystals (0.05% (w/w) in KBr) using an agate mortar and pestle until the mixture was well homogenized and then pressed into a disk with a diameter of 7 mm at 28 MPa using a hydraulic press (P-16B-027B, Riken Keiki, Tokyo, Japan) to yield a KBr tablet containing the respective species.

SR Micro FT-IR Spectroscopy. SR micro FT-IR spectroscopy was performed at the BL43IR beamline of SPring-8 (Japan Synchrotron Radiation Research Institute, Sayo, Japan) with a high-resolution microscope system (Vertex70 and Hyperion2000, Bruker Japan, Yokohama, Japan) equipped with a liquid nitrogen-cooled mercury cadmium telluride (MCT) detector and a 36× Cassegrain objective (NA = 0.5). FT-IR spectra were recorded in transmission mode as the average of 256 scans from 600 to 4000 cm^{-1} at a spectral resolution of 4 cm^{-1}, with an aperture size of 2.5 × 2.5 μm^2. The measurement points were scanned at 2.5 × 2.5 μm^2, and the number of pixels in a mapping scan depended on the array size covering the desired area of the sample. The beam path, spectrometer, microscope, and sample chamber were continuously purged with dry air to reduce the interference of CO_2 and moisture. All raw FT-IR spectra were converted to text data files using Bruker OPUS version 7.8 for further processing.

Globar Light Micro FT-IR Spectroscopy. Globar light micro FT-IR spectroscopy was performed using an IRT-7100 IR microscope with the FT/IR-4600 FT-IR spectrometer (JASCO) equipped with a high brilliant ceramic light source, liquid nitrogen-cooled single mid-band MCT detector, and 32× Cassegrain objective (NA = 0.75). FT-IR spectra were recorded in transmission mode as the average of 256 scans from 600 to 4000 cm^{-1} at a spectral resolution of 4 cm^{-1}, with an aperture size of 10 × 10 μm^2. The measurement points were scanned at 2.5 × 2.5 and 10 × 10 μm^2, and the spectra were converted to text data files using Spectra Manager version 2 (JASCO).

FT-IR Spectroscopy. *Liquid Chromatography.* The instrumental and experimental procedures are shown in Supporting Materials.

RESULTS AND DISCUSSION

Establishment of the Evaluation Method of the Chemical Distribution in a Powder. In this study, two types of chemicals, drug and additive simulants, with different

https://doi.org/10.1021/acsomega.2c07573
ACS Omega 2023, 8, 4285−4293

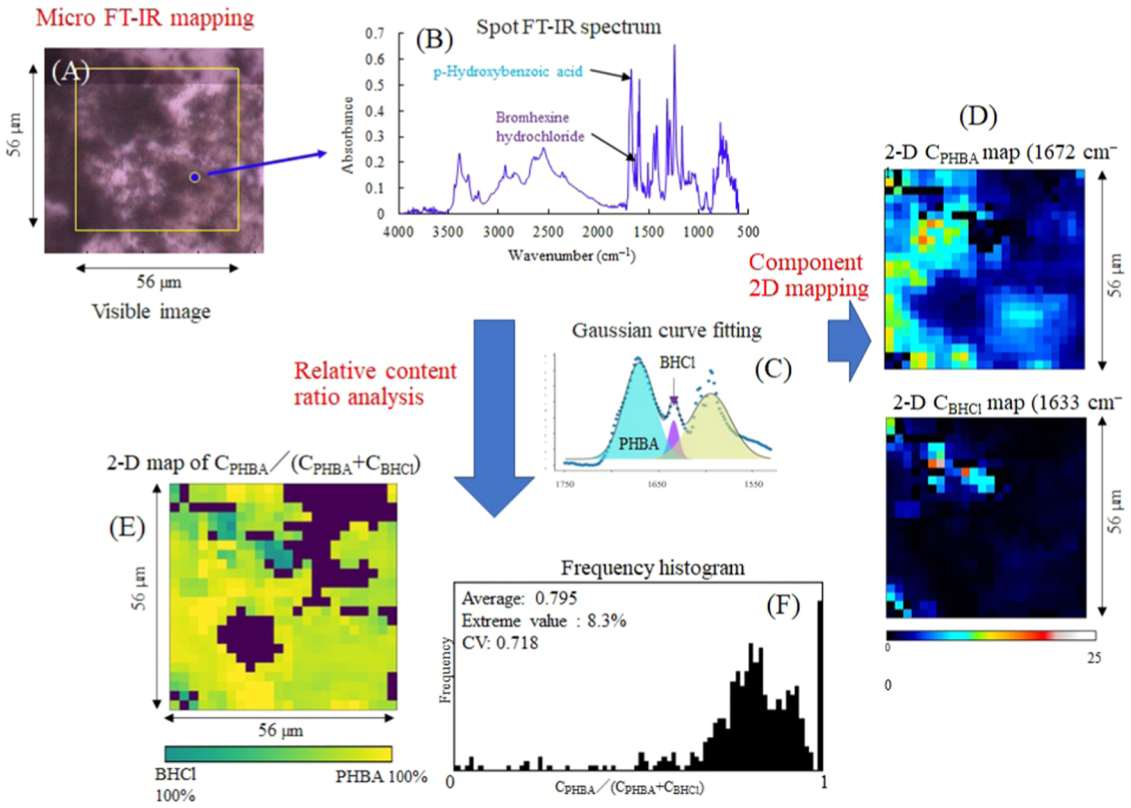

Figure 1. Schematic diagram of the flow of the analytical procedures, from micro FT-IR spectroscopy to analyzing the mixing condition. The agate mortar-homogenized powder of equal masses of bromhexine hydrochloride and *p*-hydroxybenzoic acid on a BaF_2 plate was measured via mapping analysis of micro FT-IR spectroscopy in transmission mode using the synchrotron radiation (SR) instrument with a 2.5 μm aperture and 2.5 μm step mapping of the visible image with an area of 3136 μm^2 (A). Representative FT-IR spectrum of one measuring spot (B) indicating the combination of the BHCl and PHBA spectra. The peaks of BHCl and PHBA at 1633 and 1672 cm^{-1}, respectively, are not resolved, and Gaussian curve fitting between 1750 and 1530 cm^{-1} was performed, yielding three peaks: the C═O stretching band of PHBA at 1672 cm^{-1}, N−H bending band of BHCl at 1633 cm^{-1}, and aromatic C═C stretching band of PHBA at 1606 and 1595 cm^{-1} (C). The areas of the N−H bending band of BHCl at 1633 cm^{-1} and C═O stretching band of PHBA at 1672 cm^{-1} were converted to the molar contents, shown as C_{BHCl} and C_{PHBA}, with 2D mapping shown in (D). The relative content ratio (RCR) $C_{PHBA}/[C_{BHCl} + C_{PHBA}]$ was then calculated, with 2D RCR mapping shown in (E), and the frequency histograms as vertical RCR bars at intervals of 0.0125 between 0 and 1 are shown in (F). In the plot, the average RCR, percentage of extreme values, and CV excluding the extreme values are shown.

chemical properties, were used: BHCl with aromatic amino, bromide, and aliphatic amino moieties, and PHBA with aromatic hydroxy and carboxylic moieties. Quantitative powder discrimination using mapping analysis of micro FT-IR spectroscopy should enable quantitative measurement of the target species via the target vibrational bands. The procedure is shown in Supporting Material. The areas of the vibration bands at 1633 and 1672 cm^{-1} corresponding to BHCl (C−N bending) and PHBA (C═O stretching), respectively, were measured after Gaussian curve fitting and converted to molar contents, which were represented as C_{BHCl} and C_{PHBA}, which indicate the molar amounts of the species at the measured spots. Micro FT-IR spectroscopy yields data regarding the distribution of various species within samples. 2D mapping of C_{PHBA} and C_{BHCl} yields the separate distribution patterns of PHBA and BHCl. A typical example, as measured using the SR instrument, is shown in Figure 1. The visible image (Figure 1A) almost corresponded to the 2D maps of C_{PHBA} and C_{BHCl} (Figure 1D) after merging. PHBA was observed mainly on the left-hand side of the measured area and C_{PHBA} varied depending on the measurement site. In contrast, BHCl was localized mostly in the upper left-hand-side area. The 2D distribution patterns of PHBA and BHCl clearly differed, but quantitatively estimating how the two species were mixed is challenging. Therefore, a comparison of the two relative contents should be considered. The ratio of one component to the other component (quotient: the content of one component divided by the content of the other component) is generally used in observing the specific localization of the target substance against the background substance. Inamasu et al. evaluated the distribution of chemical components of a cross section of a human hair using SR micro FT-IR spectroscopy.[22] Okada et al. evaluated the dispersion pattern of the additives in a polymer composite via micro FT-IR spectroscopy.[19] However, the use of ratios suffers from the severe drawback of an abnormal ratio (very high or infinity) observed at a denominator component content of a very low value or zero. Instead, we adopted the RCR $C_{PHBA}/[C_{BHCl} + C_{PHBA}]$ as the mixing parameter, yielding values between 0 and 1. The 2D RCR distribution map corresponding to the respective 2D maps of C_{PHBA} and C_{BHCl} (Figure 1D) is shown in Figure 1E. This map showed the absolute localization of BHCl at one spot (green) and dominant localization of BHCl (faintly yellowish-green) at small spot lines in the upper and lower left-hand-side regions, and the absolute localization of PHBA in the middle left-hand-side region (yellow) and dominant localization of PHBA in the large right-hand-side region (faintly greenish-yellow). The 2D RCR map (Figure

https://doi.org/10.1021/acsomega.2c07573
ACS Omega 2023, 8, 4285−4293

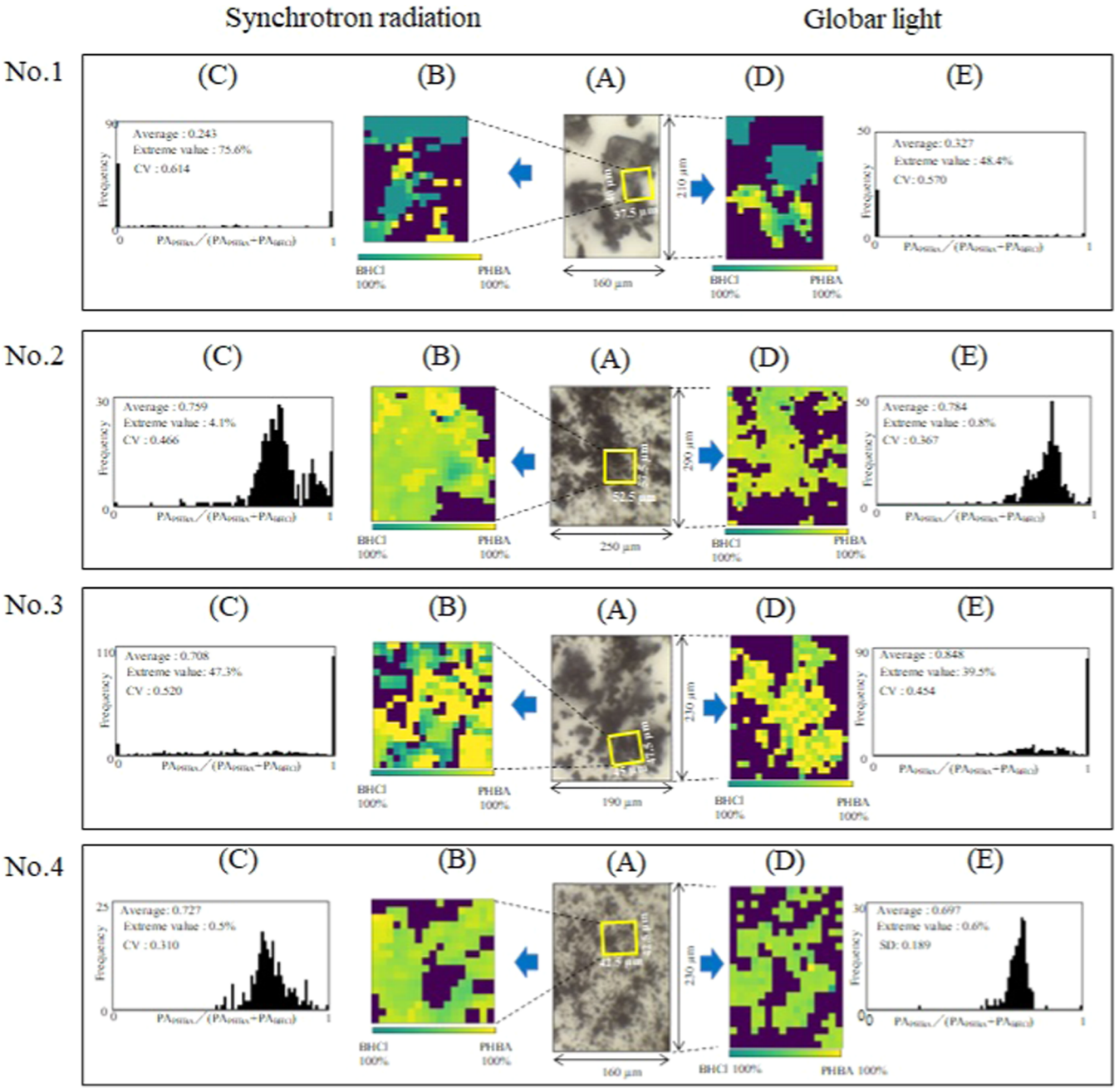

Figure 2. 2D maps and frequency histograms of the relative content ratios (RCRs) of the powders prepared via four different mixing modes. Equal masses of BHCl and PHBA powders were (No. 1) simply mixed, (No. 2) homogenized using an agate mortar, or (No. 3) dissolved in methanol and dried and then (No. 4) homogenized using an agate mortar, and the mixtures were dispersed on BaF_2 plates and subjected to micro FT-IR spectroscopy using SR and globar light instruments in transmission mode with aperture sizes of 2.5 x 2.5 and 10 x 10 μm^2 and mapping steps of 2.5 and 10 μm, respectively. Approximately 2000 and 50 000 μm^2 areas (A) were mapped via micro FT-IR spectroscopy using the SR and globar light instruments, respectively. 2D maps (B, D) and frequency histograms (C, E) of the RCRs $C_{PHBA}/[C_{BHCl} + C_{PHBA}]$ are shown, with the average RCRs, percentages of extreme values (RCR: 0, 1), and coefficients of variation (CVs) of the RCRs, excluding the extreme values. The black areas in the 2D maps are positions with no BHCl or PHBA observed.

1E) almost corresponded to the visible image (Figure 1A). To evaluate the mixing condition quantitatively, the frequency histograms of the RCRs were constructed, dividing at RCR intervals of 0.0125. If only one species exists in the measured spot, the RCR is 0 or 1, and these values are designated as extreme values. The percentage of extreme values among all of the RCR values is shown as %EV, which may be used as a mixing index. The average RCR among the histograms indicates the mixing ratio in the micro FT-IR spectroscopic measurement area. After excluding the extreme values (RCR: 0 or 1), the histograms should exhibit a well-dispersed distribution pattern. Using statistical treatment, the average RCR and standard deviation (SD) were calculated. If average RCR was <0.5, the coefficient of variation (CV) was calculated by dividing the SD by average RCR. If average RCR was >0.5, CV was calculated by dividing the SD by [1—average RCR]. CV showed the dispersity of the mixing condition. If two chemicals were mixed entirely homogeneously, the histogram

https://doi.org/10.1021/acsomega.2c07573
ACS Omega 2023, 8, 4285−4293

yielded one RCR bar. In the case of a completely homogeneous mixture of equal masses of PHBA and BHCl, an RCR of 0.75 was expected from the molecular weight ratio of 138.12 (PHBA) to 412.59 g/mol (BHCl). If two chemicals were unmixed completely, the histogram yielded only two extreme bars (RCR: 0 or 1). Depending on the mixing condition, the histograms should exhibit various patterns, as shown in Figure 1F.

In addition, for evaluating macro scale mixing conditions, LC analysis of approximately 1 mg drug powders was utilized to obtain the RCR values for the powder samples of the respective mixing modes. The %EV and the CV values were calculated, similar to the procedure for the micro FT-IR spectroscopy.

Distributions of Powders Comprising Equal Masses of Two Chemical Species Prepared Using Four Different Types of Mixing. The powder samples examined were prepared by mixing PHBA and BHCl powders using various mixing modes to yield homogeneous and inhomogeneous mixing patterns. The powder mixing conditions may indicate the manufacturing processes of seized drugs. Sample powders were prepared using equal masses of BHCl and PHBA powders by (1) simply mixing, (2) homogenizing in an agate mortar, (3) methanol dissolution and drying, or (4) homogenizing in an agate mortar after methanol dissolution-drying. The obtained samples were subjected to micro FT-IR spectroscopy to investigate the distribution patterns caused by the mixing conditions. Mixing mode (1) may correspond to a parent drug powder adulterated with additives after drug packaging, whereas mixing mode (2) may correspond to a parent drug powder adulterated with additives and sufficiently mixed prior to drug packaging. Mixing mode (3) may correspond to the inclusion of additives during parent drug manufacturing, followed by solvent evaporation and drug powder packaging. Mixing mode (4) may correspond to the inclusion of additives during parent drug manufacturing, followed by sufficient mixing of the produced materials and packaging of the resultant powder. Mixing mode (1) should result in inhomogeneous mixing with localized scattering, whereas mixing modes (2) and (4) should result in homogeneous mixing with superimposed localization. Mixing mode (3) should result in localized scattering if the two chemicals do not display strong affinities for each other or homogeneous mixing if the two chemicals display a strong affinity and form heterogeneous dimers.

Figure 2 shows the mapping results. The measurement area of the globar light instrument covered the corresponding measurement area of the SR instrument. As shown in Figure 2, No. 1, using the SR instrument, the two species appeared to be distributed inhomogeneously to yield major areas of green (100% BHCl) and yellow (100% PHBA) and a region of intermediate color in the 2D RCR map (Figure 2, No. 1(B)). The corresponding frequency histograms (Figure 2, No. 1(C)) showed a dispersed distribution pattern, with the extreme values (0 and 1 indicated in green and yellow in Figure 2, No. 1(B), respectively) exhibiting a high frequency (%EV: 76%), and the frequency bars evenly distributed between 0.0125 and 0.9875, yielding a high CV (0.61). This inhomogeneous distribution pattern did not depend on the measurement area because the patterns obtained from the measurements of the other area (Supporting Figure S5, No. 1) displayed similarly high %EV (53 and 64%) and CV (0.50 and 0.58) values, although the average RCR fluctuated (0.24, 0.42, and 0.61), deviating from the theoretical value of 0.75. Aggregates of BHCl and PHBA crystals may occupy the major region in the measurement area, with aggregates of various sizes comprising crystals containing both species in various contents. Additionally, using the globar light instrument, the two species appeared to be distributed inhomogeneously, yielding a large green (100% BHCl) region and an intermediate color pattern in the 2D RCR map (Figure 2, No. 1(D)). The corresponding frequency histograms (Figure 2, No. 1(E)) showed a dispersed distribution pattern, with the extreme value (0) exhibiting a high frequency (48%) and RCR bars evenly distributed between 0.0125 and 0.9875, yielding a high CV (0.57). This inhomogeneous distribution pattern did not depend on the measurement area because the patterns obtained from the measurements of the other areas (Supporting Figure S6, No. 1) displayed similar %EV (39 and 51%) and CV (0.51 and 0.56) values, although the average RCR fluctuated (0.19, 0.33, and 0.40) and deviated from the theoretical value of 0.75. Crystal aggregates of BHCl may occupy a large region. Generally, the distribution patterns of No. 1 mixing powder obtained using the SR and globar light instruments were similar.

As shown in Figure 2, No. 2, using the SR instrument, the two species appeared to be distributed homogeneously to yield mostly faintly yellowish-green regions and some yellow regions in the 2D RCR map (Figure 2, No. 2(B)). The corresponding frequency histograms (Figure 2, No. 2(C)) showed a homogeneous distribution pattern, with a large peak centered at RCR = 0.76, minor extreme value (RCR: 1) bar (%EV: 4%), moderate peak at RCR = 0.90, and low bars scattering from RCR = 0.7−0.3 observed, and a moderate CV (0.47). Depending on the measurement area, the distribution pattern was changeable (Supporting Figure S5, No. 2). For one measurement, the distribution pattern (Figure S5, No. 2(A), (B)) was similar to that shown in Figure 2, No. 2(B), (C). However, the frequency histograms indicated a high CV (0.72) compared to that obtained for the measurement shown in Figure 2 (CV: 0.47), probably due to rather high average RCR and low RCR bars scattering more widely from RCR = 0.7−0.0125. For the other measurement (Figure S5, No. 2(A′), (B′)), only one broad peak was observed without low bars scattering to low RCR, yielding a low CV (0.31). The average RCR was 0.62−0.80, which was similar to the theoretical value of 0.75. Mixing two separate species as powders using an agate mortar may yield incompletely homogeneous distribution at the microscopic (approximately 2.5 x 2.5 μm^2) level. Using the globar light instrument (Figure 2, No. 2), the two species appear to be distributed homogeneously to yield a wide faintly yellowish-green region in the 2D RCR map (Figure 2, No. 2(D)). The corresponding frequency histograms (Figure 2, No. 2(E)) show a homogeneous distribution pattern, with a bell-shaped peak centered at RCR = 0.78. a low %EV (0.8%) and a low CV (0.37). The homogeneous distribution pattern does not depend on the measurement area because the patterns obtained from the measurements of the other areas (Supporting Figure S6, No. 2) exhibited low %EV (0 and 3%) and CV (0.17 and 0.29) values. The average RCR was 0.69−0.81, which was similar to the theoretical value of 0.75. Mixing two separate species as powders using an agate mortar may yield a homogeneous distribution at the microscopic (approximately 10 x 10 μm^2) level.

As shown in Figure 2, No. 3, using the SR instrument, the two species appeared to be distributed inhomogeneously to

https://doi.org/10.1021/acsomega.2c07573
ACS Omega 2023, 8, 4285−4293

Table 1. Distribution Parameters Obtained Using the Different Mixing Conditions[a]

	average			percentage extreme value (%)			CV		
mixing mode	SR	globar	LC	SR	globar	LC	SR	globar	LC
1	0.423 ± 0.183	0.305 ± 0.104	0.678 ± 0.014	64.1 ± 11.3	46.0 ± 6.0	0	0.565 ± 0.057	0.613 ± 0.127	0.042
2	0.724 ± 0.094	0.760 ± 0.062	0.672 ± 0.003	4.7 ± 3.3	1.3 ± 1.7	0	0.487 ± 0.208	0.273 ± 0.100	0.008
3	0.587 ± 0.172	0.804 ± 0.063	0.676 ± 0.090	37.7 ± 13.6	23.2 ± 23.1	0	0.516 ± 0.006	0.606 ± 0.214	0.277
4	0.753 ± 0.036	0.649 ± 0.069	0.710 ± 0.011	0.3 ± 0.4	0.3 ± 0.4	0	0.341 ± 0.044	0.226 ± 0.053	0.039
1 (9:1)	0.219 ± 0.257		0.186 ± 0.021	42.3 ± 26.8		0	0.744 ± 0.402		0.113
2 (9:1)	0.277 ± 0.003		0.172 ± 0.004	5.0 ± 7.1		0	0.535 ± 0.108		0.022

[a]Mixing indices were obtained using micro FT-IR spectroscopy via frequency histogram analysis and liquid chromatography (LC). In LC, 6 powder fractions of approximately 1 mg were randomly sampled, dissolved in methanol, and analyzed to yield the relative molar contents. The average ratios are calculated using the averages of the relative content ratios (RCRs), including the extreme values (0, 1), obtained via micro FT-IR spectroscopy and LC. The percentage extreme values (%EV) are the frequency of RCR = 0 and 1. The CVs are calculated using the respective RCRs, excluding the extreme values. The micro FT-IR spectroscopy data are calculated based on Figure 2 and Supporting Figures S5−S7 for the mixed powder with a ratio of 9:1.

yield major green, yellow, and highly dispersed intermediate color regions in the 2D RCR map (Figure 2, No. 3(B)). The corresponding frequency histograms (No. 3(C)) showed an inhomogeneous distribution pattern, with the extreme values exhibiting a high frequency (%EV 47%) and the frequency RCR bars evenly distributed between RCR = 0.0125 and 0.9875, yielding a high CV (0.52). This inhomogeneous distribution pattern did not depend on the measurement area because the patterns obtained from another measurement (Supporting Figure S5, No. 3) displayed similarly high %EV (28%) and CV (0.51) values, although the average RCR fluctuated (0.71 and 0.47) close to the theoretical value of 0.75. Using the globar light instrument (Figure 2, No. 3), the two species appeared to be distributed inhomogeneously to yield a major yellow region (100% PHBA) evenly scattered over the measurement area and an intermediate color region also scattered over the 2D RCR map (Figure 2, No. 3(D)). The corresponding frequency histograms (Figure 2, No. 3(E)) showed a distribution pattern with the extreme value (RCR: 1) exhibiting a high frequency (%EV: 40%), and the RCR frequency bars formed a broad peak centered at RCR ≈ 0.8, yielding a moderate CV (0.45). Depending on the measurement area, the distribution pattern was changeable (Supporting Figure S6, No. 3). The distribution pattern (Figure S6, No. 3(A), (B)) exhibited nondispersed yellow and intermediate color regions. In the frequency histograms, a broad peak was observed at RCR = 0.76 with a low %EV (7%) and low RCR bars scattering from RCR = 0.6−0.0125, yielding a high CV (0.76). The average RCR fluctuated (0.85 and 0.76) close to the theoretical value of 0.75. During methanol evaporation from the mixed powder, BHCl and PHBA may recrystallize separately to form their respective crystal aggregates, which occupy major regions of the measurement area, yielding inhomogeneously mixed powders with various RCRs.

As shown in Figure 2, No. 4, using the SR instrument, the two species appeared to be distributed homogeneously to yield a faintly yellowish-green region in the 2D RCR map (Figure 2, No. 4(B)). The corresponding frequency histograms (Figure 2, No. 4(C)) revealed a homogeneous distribution, with a peak centered at RCR = 0.73. a low %EV (0.5%) and a low CV (0.31). The homogeneous distribution did not depend on the measurement area because the patterns obtained from another measurement (Supporting Figure S5, No. 4) exhibited no extreme values (%EV: 0) and a low CV (0.34). The average RCRs were similar (0.73 and 0.78), which were close to the theoretical value of 0.75. Mixing two species using an agate mortar after methanol dissolution may yield a homogeneous distribution at the microscopic (2.5 x 2.5 μm^2) level. Using the globar light instrument (Figure 2, No. 4), the two species appeared to be distributed homogeneously to yield a faintly yellowish-green region in the 2D RCR map (Figure 2, No. 4(D)). The corresponding frequency histograms (Figure 2, No. 4(E)) revealed a homogeneous distribution pattern, with a sharp peak centered at RCR = 0.70 a low %EV (0, 6%) and a low CV (0.19). The homogeneous distribution did not depend on the measurement area because the pattern obtained from another measurement (Supporting Figure S6, No. 4) exhibited no extreme value (%EV: 0) and a low CV (0.26). The average RCRs were similar (0.60 and 0.70), which were similar to the theoretical value of 0.75. Mixing two species using an agate mortar after methanol dissolution may yield a homogeneous distribution at the microscopic (approximately 2.5 x 2.5 μm^2) level. Generally, the distribution patterns obtained using the SR and globar light instruments were similar.

The average RCR, extreme value frequencies (%), and CVs are summarized in Table 1. The SR instrument could distinguish all of the mixing modes in %EV and CV 1 σ criteria. In contrast, the globar light instrument could not distinguish between No. 1 and No. 3 and between No. 2 and No. 4. In macro-level analysis using LC, %EVs were zero, and the CVs were small compared to those of micro FT-IR spectroscopy, and the CV for No. 3 mixing mode was higher than the other mixing modes.

Distributions of Powders Comprising Different Masses of Two Chemical Species Prepared Using Two Different Mixing Modes Measured Using an SR Instrument. In the above study, equal masses of two species were mixed, with a molar ratio of BHCl:PHBA of 1:3. We examined the effect of the mass ratio on the distribution pattern, using the SR instrument and a BHCl:PHBA mass ratio of 9:1, which was a BHCl:PHBA molar ratio of 3:1. As shown in Figure S7, following mixing mode No. 1 (simple mixing), the 2D RCR maps (B, B′) roughly corresponded to the right-hand-side regions in the visible images (A, A′). The two species appeared to be distributed inhomogeneously to yield major green (100% BHCl) and major intermediate color regions in one measurement (Figure S7, No. 1(B)) and major green region in another measurement (Figure S7, No. 1(B′)). The corresponding frequency histograms (C, C′) revealed inhomogeneous distributions, with high frequencies (23 and 61%) of the extreme values (RCR: 0). One measurement (B) yielded widely spread RCR bars evenly distributed between RCR =

https://doi.org/10.1021/acsomega.2c07573
ACS Omega 2023, 8, 4285−4293

0.0125 and 0.9875, and the other revealed a peak centered at RCR = 0.05 and widely spread bars from RCR = 0.5−0.0125. The CVs were 0.46 and 1.03, and the average RCR also fluctuated highly (0.40 and 0.04), however roughly close to the theoretical value of 0.25. Aggregates of BHCl and PHBA crystals may occupy the major region of the measurement area, yielding varied RCRs within the inhomogeneously mixed powders.

Using mixing mode No. 2 (homogenization using an agate mortar, Figure S7), the 2D RCR map (B) almost corresponded to the visible image in one measurement (A), but this was not the case in the other measurement (B′, A′). The two species appeared to be distributed almost homogeneously, yielding broadened color patterns in the 2D RCR maps (Figure S7, No. 2(B), (B′)). The frequency histograms of one measurement (Figure S7, No. 2(C)) revealed that the extreme value (RCR: 0) exhibited a minor frequency (%EV: 10%) and the bars formed a wide peak centered at RCR = 0.28 with a tail to RCR = 0.8, yielding a high CV (0.61). In the other measurement, the frequency histograms (Figure S7, No. 2(C′)) formed a flattened peak centered at RCR ≈ 0.3, yielding a moderate CV (0.46). The average RCR was a reproducible 0.28, which was similar to the theoretical value of 0.25. Mixing two species using an agate mortar may yield a homogeneous distribution at the microscopic (approximately 10 x 10 μm^2) level.

Effect of the Analyzing Window Size on the Distribution Pattern. As shown in Figure S8, the micro FT-IR spectroscopic data (Figures 2 and S5) were reanalyzed after widening the analyzing window size from the original 1-fold (2.5 × 2.5 μm^2 measuring area, black square shown in the upper left of Figure S8Aa) to 4-fold (5 × 5 μm^2 analyzing area, blue square shown in the upper left of Figure S8Aa,c) and 16-fold (10 × 10 μm^2 analyzing area, red square shown in the upper left of Figure S8Aa,c,e) analyzing areas. Due to limited data points, only 4- and 16-fold-widened analyses were performed, with higher-fold analyses not conducted. Using the SR instrument, window widening yielded 2D RCR maps that exhibited coarse distribution profiles, although the distribution patterns were similar. The frequency histograms revealed a peak that sharpens as the measurement area increased from 1- to 4-fold, resulting in the reduction of %EV from 4% to zero. Additionally, using the globar light instrument, the same pattern was observed. A reduction in the CV (0.37−0.25) was also observed with the increase in window size. Using a similar approach, Okada et al. reported that the CVs decreased with the window size, depending on the distribution pattern, with a more inhomogeneously distributed sample of polyethylene/cellulose nanofiber composites yielding a high CV with a narrower window size.[19]

These analyses with wider measuring windows were performed for the other mapping examinations (Figures 2 and S5 and S6), and the %EV and CV values were plotted as functions of the window size (Figures S9 and S10). For mixing mode No. 1 (simple mixing), the %EV values gradually decreased, with a large gap observed at a window size of 10 μm between the results obtained using the SR and globar light instruments. For mixing mode No. 3 (methanol dissolution and drying), the moderate %EV gradually decreased to zero, with a large gap observed at a window size of 10 μm between the results obtained using the SR and globar light instruments. Large gaps of the %EV between the SR and globar light instruments for mixing modes No. 1 and No. 3 at 10 μm window size may be due to lowered analyzing accuracy in the SR instrument as the analyzing points were too few (15−38) compared to those in the globar light instrument (220−437). Finally, the %EV reached zero at a macro window size, as determined using liquid chromatography. The %EV values obtained using No. 1 were higher than those obtained using No. 3, regardless of window size. For mixing mode No. 2 (homogenization using an agate mortar), the low %EV values reached zero, with only a small gap observed at a window size of 10 μm between the results obtained using the SR and globar light instruments. For mixing mode No. 4 (homogenization using an agate mortar after methanol dissolution), the almost-zero %EV remained. The %EV observed using the No. 3 mode was equal to or higher than that observed using the No. 4 mode, regardless of window size. Only at a window size of 2.5 μm, all four mixing modes may be differentiated from each other by the %EV values, and at a window size of 5−10 μm, all but the combination of No. 2/No. 4 may be differentiated. Using a window size of >20 μm, only No. 1 may be differentiated from the other mixing modes.

As commercial reagents, the BHCl and PHBA powders comprised aggregated crystals with sizes of >100 μm, according to optical microscopy (data not shown), and thus, No. 1 powder could be distinguished from No. 2 powder, which was microscopically observed as crystals with sizes of approximately 10 μm. No. 3 powder may comprise few micrometer-level recrystallized components, and thus, No. 4 powder does not exhibit single-component spots using a window size of >20 μm. After crushing the crystal aggregates of No. 1 and No. 3 powders, the corresponding homogenized No. 2 and No. 4 powders exhibit no purely single-component spots (extreme value points) using a window size of >5 μm.

For the No. 1 powder, the high CVs gradually increased to constant high CVs. For powder No. 3, the high CVs gradually increased or decreased to stable high CVs (approximately 0.6). The difference in the CVs of the No. 1 and No. 3 powders varied with window size, although they were high and fluctuated over the range of measuring window sizes but decreased to low values at macro window sizes (milligram level), according to liquid chromatography. A moderate CV might be obtained at the macro window level for the No. 3 powder because large crystallized solids might be formed to yield an inhomogeneous distribution at the macro level during methanol evaporation. In contrast, the CVs of the No. 2 and No. 4 powders decreased gradually, finally reaching zero at a macro window size. The difference in the CVs of the No. 2 and No. 4 powders decreased with the measuring window size. Among the four mixing modes, the CVs of No. 1, No. 2, and No. 3 powders were similar at a window size of 2.5 μm, indicating that at 2.5 μm, two different types of crystals (BHCl and PHBA) and related crystal aggregates appear to be distributed inhomogeneously, with only the No. 4 powder displaying a homogeneous distribution. At measuring window sizes of 5−10 μm, the distribution of methanol dissolved and dried No. 2 powder gradually became homogeneous and could not be differentiated from the No. 4 powder. Using a window size of >10 μm, the No. 1 and No. 3 powders may be easily differentiated from the No. 2 and No. 4 powders.

Mixing using an agate mortar could provide only crystalline-level mixing over a space of a few tens of micrometers, but not amorphous mixing. BHCl yielded orthorhombic crystals,[36] and based on visible microscopy, several micrometer-sized colorless rectangular crystals and particles with sizes of several tens of micrometers were observed in the commercial BHCl powder.

https://doi.org/10.1021/acsomega.2c07573
ACS Omega 2023, 8, 4285−4293

When homogenized using an agate mortar, the crystals should be crushed to form particles with sizes of approximately 1 μm. These particles should be aggregated to form clusters with sizes of between several micrometers and more than several hundred micrometers (data not shown). PHBA yielded monoclinic crystals,[37] and based on visible microscopy, several micrometer-sized colorless rice grain-like crystals and particles with sizes of several tens of micrometers were observed in the commercial PHBA powder. When homogenized using an agate mortar, ~10 μm-sized rice grain-like crystals and aggregated large clusters were observed (data not shown). Based on optical microscopy of the mixed powders (No. 1−No. 4), particles and their aggregates, with respective sizes of 1−2 and 5−15 μm, were observed (data not shown). Differentiating these mixed powders using optical microscopy was impossible. Therefore, considering regular crystal sizes of tens of micrometers, recrystallized crystal sizes of several micrometers, and the capacity of agate mortar to yield homogeneous mixing over a space of several tens of micrometers, differentiation among the No. 1−No. 4 powders should be possible using the SR instrument with an intense light source resulting in high apparent spatial resolution by evaluating %EV and CV, and differentiation between the No. 2 and No. 4 powders using the globar light instrument with a lower apparent spatial resolution should be impossible. For differentiation over a space of several micrometers, the SR instrument is superior to the globar light instrument, and this superiority may contribute to the discrimination of powdered drugs.

CONCLUSIONS

In this study, a quantitative method was successfully established to evaluate the mixing conditions of two simulated drugs, BHCl and PHBA, in powders subjected to SR and globar light micro FT-IR spectroscopy. The RCR obtained from the corrected areas of vibration peaks specific to the respective drugs was adopted as a mixing parameter, with the corresponding 2D map qualitatively revealing the distribution pattern. The frequency histograms were plotted against RCR to quantitatively evaluate the mixing condition of the two species. Using the percentage of the extreme values (exclusively one component present: RCR = 0 and 1) and CV (if average RCR was >0.5, CV was calculated using the SD divided by (1—average RCR)) of the frequency after excluding the extreme values, the mixing condition could be quantitatively analyzed among the four mixing modes: simple mixing (No. 1), agate mortar homogenization (No. 2), methanol solubilization and drying (No. 3), and methanol dissolution and drying followed by homogenization (No. 4). The %EV and CV values of mixing mode No. 1 and No. 3 were >20 and >0.5%, whereas those of No. 2 and No. 4 were <5 and <0.5%. The SR instrument could distinguish all of the mixing modes in %EV and CV 1 σ criteria. In contrast, the globar light instrument could not distinguish between No. 1 and No. 3 and between No. 2 and No. 4. Especially, superior apparent spatial resolution by the SR instrument should achieve the discrimination between No. 2 and No. 4, where spatial resolution is close to the target drug crystal size. Plotting of the window size confirmed the changes in %EV and CV when using the micron and macro window sizes, depending on the mixing modes. Therefore, micro FT-IR spectroscopy of the drug powder and subsequent quantitative evaluation using the RCR frequency histograms may distinguish drug powders with the same constituents prepared under different mixing conditions in various manufacturing processes.

ASSOCIATED CONTENT

Supporting Information

The Supporting Information is available free of charge at https://pubs.acs.org/doi/10.1021/acsomega.2c07573.

Forensic discrimination of drug powder based on drug mixing condition determined using micro Fourier transform infrared microspectroscopy (PDF)

AUTHOR INFORMATION

Corresponding Author

Yasuo Seto − *RIKEN SPring-8 Center, Sayo-gun, Hyogo 679-5148, Japan;* orcid.org/0000-0002-0983-4162; Email: seto.y@spring8.or.jp

Authors

Takahiro Iwai − *RIKEN SPring-8 Center, Sayo-gun, Hyogo 679-5148, Japan;* Present Address: Research & Development Group, Hitachi, Ltd., 1-280, Koigakubo, Kokubunji-shi, Tokyo 185-8601, Japan

Sadao Honda − *Japan Synchrotron Radiation Research Institute, Sayo-gun, Hyogo 679-5198, Japan*

Shimpei Watanabe − *RIKEN SPring-8 Center, Sayo-gun, Hyogo 679-5148, Japan*

Ritsuko Matsushita − *RIKEN SPring-8 Center, Sayo-gun, Hyogo 679-5148, Japan*

Toshio Nakanishi − *RIKEN SPring-8 Center, Sayo-gun, Hyogo 679-5148, Japan*

Masahisa Takatsu − *RIKEN SPring-8 Center, Sayo-gun, Hyogo 679-5148, Japan*

Taro Moriwaki − *Japan Synchrotron Radiation Research Institute, Sayo-gun, Hyogo 679-5198, Japan*

Makina Yabashi − *RIKEN SPring-8 Center, Sayo-gun, Hyogo 679-5148, Japan;* orcid.org/0000-0002-2472-1684

Tetsuya Ishikawa − *RIKEN SPring-8 Center, Sayo-gun, Hyogo 679-5148, Japan*

Complete contact information is available at: https://pubs.acs.org/10.1021/acsomega.2c07573

Notes

The authors declare no competing financial interest.

ACKNOWLEDGMENTS

The studies at SPring-8 (BL43IR) were performed with the approval of the Japan Synchrotron Radiation Research Institute (Proposal Nos. 2019B1279; 2020A1326; 2021A1247; 2021B1328; 2022A1208). This work was supported by KAKENHI Grant-in-Aid for Scientific Research (B; grant no. 22H01732) from the Japan Society for the Promotion of Science.

REFERENCES

(1) World Health Organization. Drugs (psychoactive), 2022. https://www.who.int/health-topics/drugs-psychoactive#tab=tab_1.

(2) Drummer, O.; Gerostamoulos, D.Forensic Drug Analysis. In *Forensic Drug Analysis*; Drummer, O.; Gerostamoulos, D., Eds.; Future Science: London, Great Britain, 2013; Chapter 1, pp 3−9.

(3) Inoue, H.; Iwata, Y. T.; Kuwayama, K. Characterization and profiling of methamphetamine seizures. *J. Health Sci.* **2008**, *54*, 615−622.

(4) Iwata, Y. T.; Kuwayama, K.; Tsujikawa, K.; Kanamori, T.; Inoue, H. Profiling of methamphetamine. *Bunseki Kagawa* **2014**, *63*, 221−231.
(5) Kobayashi, K.; Iwata, T. Y.; Kanamori, T.; Inoue, H.; Kishi, T.*Analysis of Impurities in Methamphetamine and Impurity Profiling*; National Research Institute of Police Science, 2000; Vol 53, 1−9.
(6) Ricci, C.; Eliasson, C.; Macleod, N. A.; Newton, P. N.; Matousek, P.; Kazarian, S. G. Characterization of genuine and fake artesunate anti-malarial tablets using Fourier-transform infrared imaging and spacially offset Raman spectroscopy through blister packs. *Anal. Bioanal. Chem.* **2007**, *389*, 1523−1532.
(7) Adams, F.; Barbante, C. History and present status of imaging analysis. *Talanta* **2012**, *102*, 16−29.
(8) Steiner, G.; Koch, E. Trends in Fourier transform infrared spectroscopic imaging. *Anal. Bioanal. Chem.* **2009**, *394*, 671−678.
(9) Kuzuhara, A.; Hori, T. Reduction mechanism of -cycteine on keratin fibers using microspctrophotometry and Raman spectrometry. *Biopolymer* **2005**, *79*, 324−334.
(10) Ewing, A. V.; Kazarian, S. G. Infrared spectroscopy and spectroscopic imaging in forensic science, critical review. *Analyst* **2017**, *142*, 257−272.
(11) Ricci, C.; Phiriyavityopas, P.; Curum, M.; Chan, L. L. A.; Jickells, S.; Kazarian, S. G. Chemical imaging of latent fingerprint residues. *Appl. Spectrosc.* **2007**, *61*, 514−522.
(12) Banas, A.; Banas, K.; Breese, M. B. H.; Loke, J.; Lim, S. K. Spectroscopic detection of exogenous materials in latent fingerprints treated with powders and lifted off with adhesive tapes. *Anal. Bioanal. Chem.* **2014**, *406*, 4173−4181.
(13) Lanzarotta, A.; Lakes, K.; Marcott, C. A.; Witkowski, M. R.; Somme, A. J. Analysis of counterfeit pharmaceutical tablet cores utilizing macroscopic infrared spectroscopy and infrared spectroscopic Imaging. *Anal. Chem.* **2011**, *83*, 5972−5978.
(14) Ricci, C.; Chan, K. L. A.; Kazarian, S. G. Combining the tape-lift method and Fourier transform infrared spectroscopic imaging for forensic applications. *Appl. Spectrosc.* **2006**, *60*, 1013−1021.
(15) Lanzarotta, A. Analysis of forensic casework utilizing infrared spectroscopic imaging. *Sensors* **2016**, *16*, No. 278.
(16) Banas, K.; Banas, A.; Moser, H. O.; Bahou, M.; Li, W.; Yang, P.; Cholewa, M.; Lim, S. K. Multivariate analysis techniques in the forensic investigation of the postblast residues by means of Fourier transform-infrared spectroscopy. *Anal. Chem.* **2010**, *82*, 3038−3044.
(17) Yonemochi, E.; Furuyama, N.; Bunko, M.; Moriwaki, T.; Ikemoto, Y.; Terada, K. Evaluation of dispersion state of the two racemic compounds of troglitazone in pharmaceutical granules using IR-to-Thz imaging. *Infrared Phys. Technol.* **2008**, *51*, 450−453.
(18) Shinzawa, H.; Mizukado, J.; Kazarian, S. G. Fourier Transform Infrared (FT-IR) Spectroscopic imaging analysis of partially miscible PMMA−PEG blends using two-dimensional disrelation mapping. *Appl. Spectrosc.* **2017**, *71*, 1189−1197.
(19) Okada, K.; Muroga, S.; Ohshima, M. FT-IR imaging as a new method to evaluate the dispersion of additives. *Kobunshi Ronbunsyu* **2018**, *75*, 212−220.
(20) de Oliveira, R. R.; de Juan, A. Design of heterogeneity indeces for blending quality assessment based on hyperspectral images and variographic analysis. *Anal. Chem.* **2020**, *92*, 15880−15889.
(21) Ikemoto, Y.; Moriwaki, T.; Okamura, H.; Sasaki, T.; Yoneyama, N.; Taguchi, A.; Inouye, Y.; Kawata, S.; Kinoshita, T. Broad band infrared near-field spectroscopy at finger print region using SPring-8. *Infrared Phys. Technol.* **2008**, *51*, 417−419.
(22) Inamasu, S.; Moriwaki, T.; Ikemoto, Y. Analysis of human hair cross section using infrared microspectroscopy. *J. Soc. Cosmet. Chem. Jpn.* **2016**, *50*, 209−217.
(23) Maric, M.; van Bronswijk, W.; Lewis, S. W.; Pitts, K. Synchrotron FTIR characterization of automotive primer surfacer paint coatings for forensic purposes. *Talanta* **2014**, *118*, 156−161.
(24) Kempson, I. M.; Kirkbridge, K. P.; Skinner, W. M.; Coumbaros, J. Applications of synchrotron radiation in forensic trace evidence analysis. *Talanta* **2005**, *67*, 286−303.
(25) Miller, L. M.; Dumas, P. Chemical imaging of biological tissue with synchrotron infrared light, Review. *Biochim. Biophys. Acta, Biomembr.* **2006**, *1758*, 846−857.
(26) Vernoud, L.; Bechtel, H. A.; Martin, M. C.; Reffner, J. A.; Blackledge, R. D. Characterization of multilayered glitter particles using synchrotron FT-IR microscopy. *Forensic Sci. Int.* **2011**, *210*, 47−51.
(27) Surowka, A. D.; Adamek, D.; Sczerbowska-Boruchowska, M. The combination of artificial neural networks and synchrotron radiation-based infrared micro-spectroscopy for a study on the protein composition of human glial tumors. *Analyst* **2015**, *140*, 2428−2438.
(28) Dorakumbura, B. N.; Boseley, R. E.; Becker, T.; Martin, D. E.; Richter, A.; Tobin, M. J.; van Bronswjik, W.; Vongsvivut, J.; Hackett, M. J.; Lewis, S. W. Revealing the spatial distribution of chemical species within latent fingermarks using vibrational spectroscopy. *Analyst* **2018**, *143*, 4027−4039.
(29) Dumas, P.; Tobin, M. J. A bright source for infrared microspectroscopy: synchrotron radiation. *Spectrosc. Eur.* **2003**, *15*, 17−23.
(30) Miller, L. M.; Smith, R. J. Synchrotron versus globars, point-detectors versus focal plane arrays: Selecting the best source and detector for specific infrared microspectroscopy and imaging applications. *Vib. Spectrosc.* **2005**, *38*, 237−240.
(31) Levenson, E.; Lerch, P.; Martin, M. V. Infrared imaging; Synchrotrons vs. arrays, resolution vs. speed. *Infrared Phys. Technol.* **2006**, *49*, 45−52.
(32) Levenson, E.; Lerch, P.; Martin, M. C. Spatial resolution limits for synchrotron-based spectromicroscopy in the mid- and near-infrared. *J. Synchrotron Radiat.* **2008**, *15*, 323−328.
(33) Moriwaki, T.; Ikemoto, Y. BL43IR at SPring-8 redirected. *Infrared Phys. Technol.* **2008**, *51*, 400−403.
(34) Andrew Chan, K. L.; Kazarian, S. G. Attenuated total reflection Fourier-transform infrared (ATR-FTIR) imaging of tissues and live cells. *Chem. Soc. Rev.* **2016**, *45*, 1850−1864.
(35) Vongsvivut, J.; Truong, V. K.; Al Kobaisi, M.; Maclaughlin, S.; Tobin, M. J.; Crawford, R. J.; Ivanova, E. P. Synchrotron macro ATR-FTIR microsoectroscopic analysis of silica nanoparticle-embedded polyester coated steel surfaces subjected to prolonged UV and humidity exposure. *PLoS One* **2017**, *12*, No. e0188345.
(36) Koo, C. H.; Jung, Y. J.; Lee, S. W. The crystal and molecular structure of bromhexine·HCl. *Arch. Pharm. Res.* **1984**, *7*, 115−120.
(37) Heath, E. A.; Singh, P.; Ebisuzaki, Y. Structure of *p*-hydroxybenzoic aid and *p*-hydroxybenzoic acid-acetone complex. *Acta Crystallogr., Sect. C: Cryst. Struct. Commun.* **1992**, *48*, 1960−1965.

https://doi.org/10.1021/acsomega.2c07573
ACS Omega 2023, 8, 4285−4293